

Hollow Silica Spheres Embedded in a Porous Carbon Matrix and Its Superior Performance as the Anode for Lithium-Ion Batteries

Xi Cao, Xiuyun Chuan, Shuang Li, Dubin Huang, and Guozhong Cao*

Silica (SiO_2) is regarded as one of the most promising anode materials for lithium-ion batteries due to the high theoretical specific capacity and extremely low cost. However, the low intrinsic electrical conductivity and the big volume change during charge/discharge cycles result in a poor electrochemical performance. Here, hollow silica spheres embedded in porous carbon (HSS-C) composites are synthesized and investigated as an anode material for lithium-ion batteries. The HSS-C composites demonstrate a high specific capacity of about 910 mA h g^{-1} at a rate of 200 mA g^{-1} after 150 cycles and exhibit good rate capability. The porous carbon with a large surface area and void space filled both inside and outside of the hollow silica spheres acts as an excellent conductive layer to enhance the overall conductivity of the electrode, shortens the diffusion path length for the transport of lithium ions, and also buffers the volume change accompanied with lithium-ion insertion/extraction processes.

(1961 mA h g^{-1}), and extremely low cost.^[9,10] However, as a common issue of SiO_2 and other metal oxides anodes, the majority of the capacity is delivered at potentials higher than 1.0 V versus Li/Li⁺, which is different from the silicon anodes.^[9–14] Also, some intrinsic drawbacks for SiO_2 as an electrode material including poor electrical conductivity and low initial Coulombic efficiency limit the electrochemical performance.^[10,11,15–18] Incorporating silica with carbon has been demonstrated as one promising approach to circumvent the poor electrical conductivity and large volume variation during the charge–discharge processes.^[11,19] By soaking nanosized silica (with a diameter of about 7 nm) in sucrose solution and then heat treated at $900 \text{ }^\circ\text{C}$ under nitrogen atmosphere, a C- SiO_2 composite with

50.1% SiO_2 prepared by Yu and co-workers delivered a capacity of about 550 mA h g^{-1} .^[19] Another C- SiO_2 composite with both porous carbon and silica bicontinuous nanostructure was prepared via a simple sol–gel method and delivered a reversible specific capacity of 560 mA h g^{-1} .^[11] Except the relatively lower capacitance, more concern is that charge–discharge tests of both C- SiO_2 composites were performed at a relatively low current density of 50 mA g^{-1} , which is hardly to meet the application demands for the high rate performance LIBs. Higher capacity could be obtained by refined designing and incorporating tailored void space, for example, Yan et al.^[9] reported that the SiO_2 porous nanocubes with a hollow structure exhibited a reversible capacity of 919 mA h g^{-1} at a current density of 100 mA g^{-1} , and SiO_2 nanotubes synthesized by a two-step hard-template method exhibited a stable reversible capacity of 1266 mA h g^{-1} after 100 cycles at a current density of 50 mA g^{-1} .^[20] However, the high cost, low packing density, and low current density still limit the practical application of these materials.

By preparing C- SiO_2 composites with controlled nanostructure in a facile method, it can be assumed that the capacity of silica-based anode material still has a large potential to be enhanced. In this work, hollow silica spheres embedded in porous carbon (HSS-C) was developed by utilizing tetraethoxysilicate (TEOS) and resol ($[\text{C}_6\text{H}_3\text{OHCH}_2]_n$, $M_w < 500 \text{ g mol}^{-1}$)^[21] as SiO_2 and carbon sources, respectively. The hollow silica spheres were completely confined in the electrical conductive continuous porous carbon framework with a large surface area and void space that can buffer the volume change

1. Introduction

Lithium-ion batteries (LIBs) have attracted tremendous interest as energy storage devices to power portable electronics and electrical vehicles, and for stationary storage due to their high energy density and long cycle life.^[1–5] As a most promising anode material for the next generation of lithium-ion batteries, silicon has received a lot of attention recently mainly due to its highest specific capacity of 4200 mA h g^{-1} .^[6] However, the drastic volume change of Si (>300%) leads to an unacceptable capacity fading during repeated insertion and extraction of lithium ions (Li⁺) and significantly limits its commercial application.^[6–8]

More recently, silica (SiO_2) is drawing an increasing attention as an alternative candidate due to the less volume change during cycling because of the in situ formation of passivation secondary phase, relatively high theoretical specific capacity

X. Cao, Prof. X. Chuan, D. Huang
School of Earth and Space Science
Peking University
Beijing 100871, P. R. China

X. Cao, S. Li, Prof. G. Cao
Department of Materials Science and Engineering
University of Washington
Seattle, WA 98195, USA
E-mail: gzcao@u.washington.edu



DOI: 10.1002/ppsc.201500218

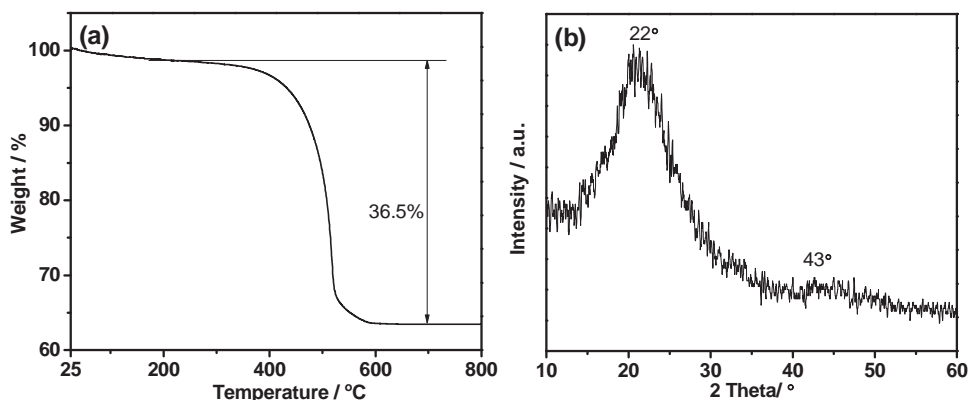


Figure 1. a) TGA curve of carbon coated hollow silica spheres composite (HSS-C) from 25 to 800 °C at a heating rate of 10 °C min⁻¹ in a flow air and b) XRD pattern of carbon coated hollow silica spheres composite (HSS-C).

during lithium-ion insertion/extraction processes, leading to an enhanced specific capacity and a good cyclic performance at a relative high current density of 200 mA g⁻¹.

2. Results and Discussion

The SiO₂ content in the HSS-C sample is determined to be about 63.5 wt% by thermogravimetric (TGA), as shown in **Figure 1a**. The X-ray diffraction (XRD) pattern of sample HSS-C shown in **Figure 1b** demonstrates no distinct diffraction peaks, suggesting the amorphous nature of the powders, with a broad and weak diffraction peak located in the 2θ range of 21–23° associated with amorphous SiO₂ and the weak peak around 43° assigned to carbon.^[10] No silicon peak is found, demonstrating no SiO₂ was reduced to Si, as surely SiO₂ cannot be reduced to Si or SiC by carbon at temperatures below 1000 °C.^[10]

Figure 2 presents a general view of the morphologies of the hollow silica spheres (HSS) and the HSS-C composites. Silica spheres with smooth surface were prepared after the removal of polystyrene (PS) spheres, and the silica spheres exhibit a uniform size (about 350 nm in diameter) and a hollow structure (about 200 nm in diameter, which is almost equal to the diameter of PS spheres, as shown in **Figure S1**, Supporting Information), with a thickness of silica to be 75 nm (**Figure 2a**). After the impregnation of an ethanol solution of resol and P123,

evaporating ethanol, thermosetting at 100 °C and carbonizing, the hollow silica spheres were embedded in carbon matrix and formed the HSS-C, as shown in **Figure 2b**.

As the hollow silica spheres were dispersed and embedded in the porous carbon matrix, it was not a uniform coating, and the thickness of the porous carbon outside the SiO₂ spheres may differ from different directions. As shown in **Figure 3a,b**, the carbon on the SiO₂ spheres has a different thicknesses and shows a porous structure.

Nitrogen sorption isotherms were used to determine the porous structure of the HSS and HSS-C. **Figure 4** gives their nitrogen sorption isotherms and the pore size distribution (based on the Barrett–Joyner–Halenda (BJH) desorption analyses). The HSS shows a type-IV isotherm (**Figure 4a**) with a rapid increase of adsorption quantity in high relative pressure, with relatively a wide pore size distribution from 3 to 150 nm (**Figure 4b**), suggesting the existence of mesopores and macropores. The mesopores may mainly come from the nanopores between the SiO₂ particles, while the macropores may due to the aggregates of primary spheres and the hollow pores in the silica spheres. The Brunauer–Emmett–Teller (BET) derived surface area is determined to be 68.6 m² g⁻¹ (with the average particle size of SiO₂ calculated to be about 33 nm, as listed in the Supporting Information), and a total pore volume of 0.530 cm³ g⁻¹. In comparison, HSS-C exhibits a type IV isotherm with a typical H2 type hysteresis loop (**Figure 4c**), suggesting the existence of

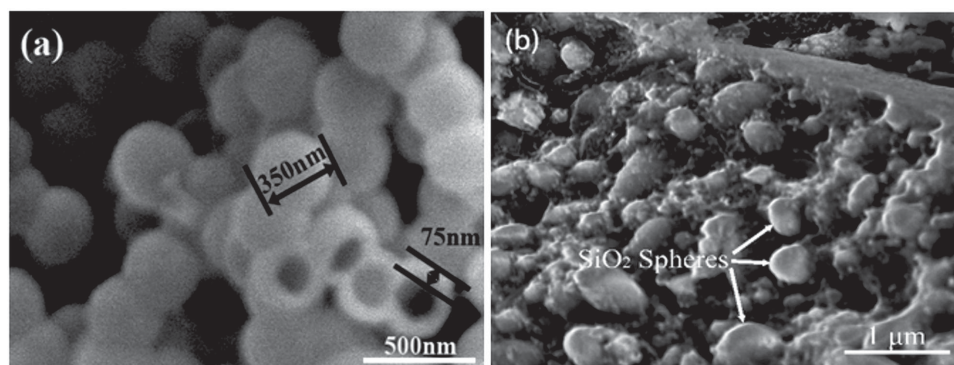


Figure 2. Field-emission scanning electron microscopy (FESEM) images of a) the hollow SiO₂ spheres (HSS) and b) the hollow SiO₂ spheres embedded in carbon (HSS-C).

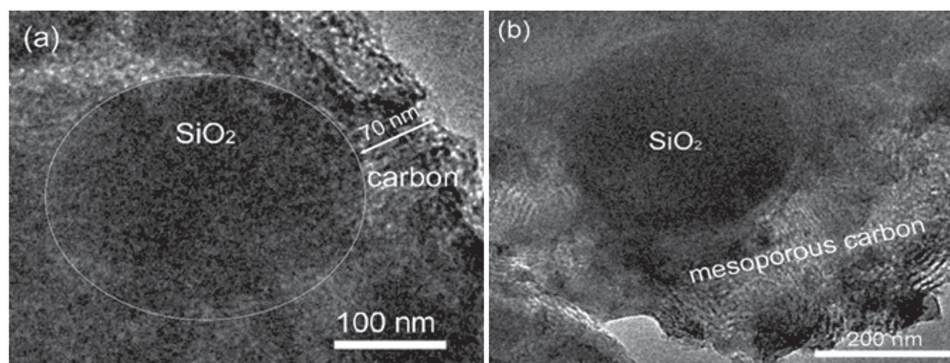


Figure 3. a,b) Transmission electron microscopy (TEM) images of the hollow SiO_2 spheres embedded in carbon (HSS-C).

mainly mesopores, which are due to the mesoporous carbon.^[22] The BET surface area and total pore volume are calculated to be $297 \text{ m}^2 \text{ g}^{-1}$ and $0.315 \text{ cm}^3 \text{ g}^{-1}$, respectively, with a maximum pore size distribution peak at 4 nm (Figure 4d). The decrease of pore volume and the increase of BET surface area are mainly due to the carbon filling of the HSS pores.

The cyclic voltammetry (CV) curves of HSS-C sample at a scanning rate of 0.1 mV s^{-1} in the voltage range of 0.01–2.8 V are displayed in Figure 5a. The reduction peaks located at 1.37 and 0.75 V appeared in the first cycle only. The peak at 1.37 V is believed to result from the decomposition of vinylene carbonate (VC), the additive in the electrolyte.^[23] This cathodic peak at 0.75 V is associated with the electrolyte decomposition and the formation of solid electrolyte interface (SEI) layer on

the surface of the electrode.^[19,24–27] The formation of SEI film in the first cycle is through irreversible reactions, which may result in the low Coulombic efficiency and loss in the charge capacity. These peaks are not observed in the subsequent cycles, indicating the formation of SEI is mostly complete in the first cycle. The following sloping region should be assigned to the electrochemical reduction of SiO_2 to Si and the irreversible formation of Li_2O or Li_4SiO_4 ; the reversible reaction of Li both Si and carbon.^[11,16,19,28] The first three charge and discharge profiles of mesoporous carbon are also shown in Figure S2a (Supporting Information), which also shows an obvious discharge plateau from 0.75 to 0.01 V. Both Si and carbon would alloy/dealloy with lithium reversibly and provides the reversible capacity (Reaction (2) and (3)):

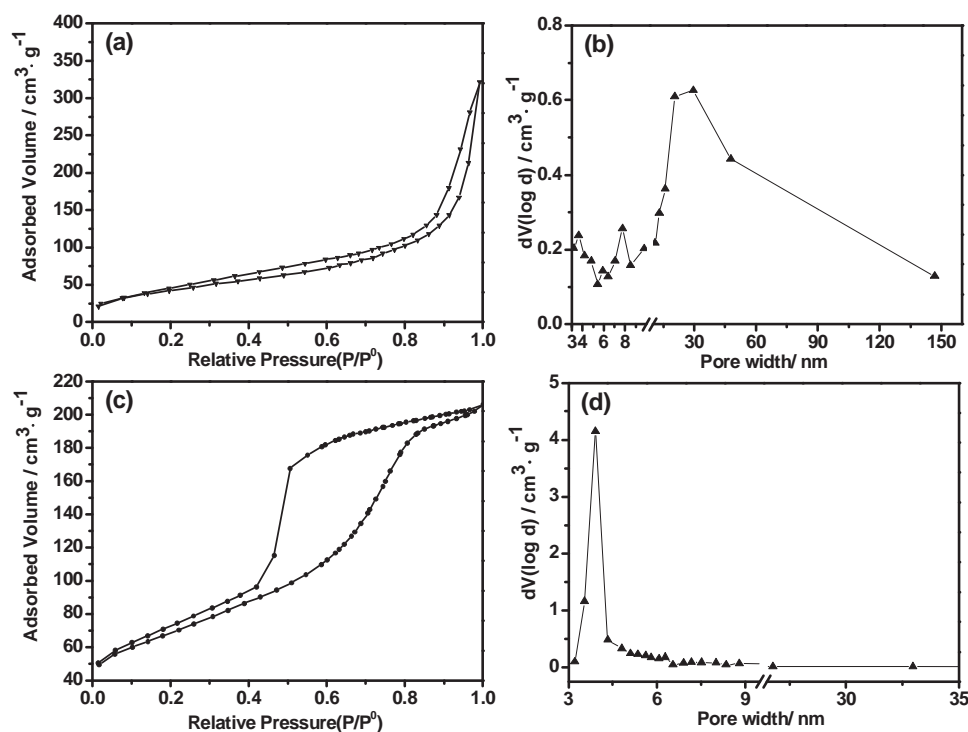


Figure 4. Nitrogen adsorption–desorption isotherms of a) HSS and c) HSS-C and the corresponding BJH desorption pore size distribution of b) HSS and d) HSS-C.

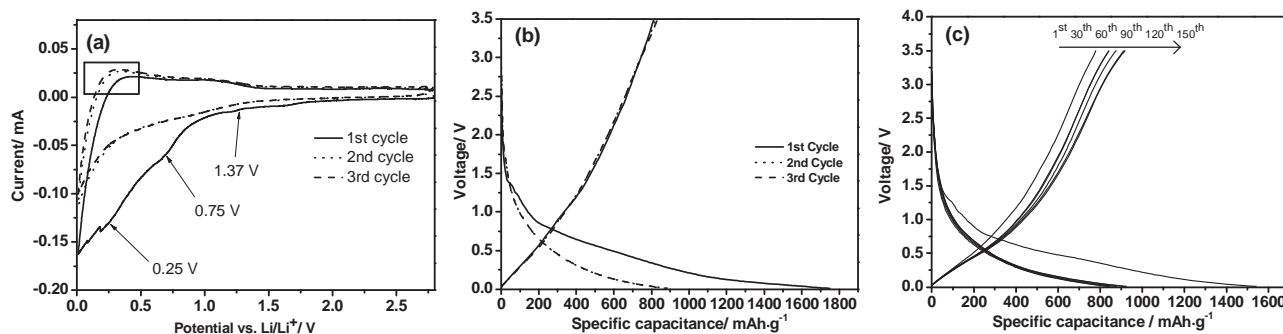
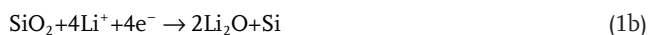
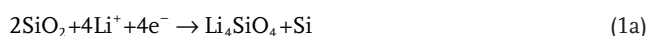


Figure 5. a) The CV curves of HSS-C electrode measured in the voltage range of 0.01–2.8 V (vs Li/Li⁺) with a scan rate of 0.1 mV s⁻¹; b) first three discharge and charge curves of the HSS-C electrode at a current density of 100 mA g⁻¹; and c) discharge and charge curves of the HSS-C electrode versus different cycles at a current density of 200 mA g⁻¹.



The anodic peak occurs at 0.33 V in the first cycle can be attributed to dealloying of Li from Si. This peak becomes distinct and shifts to a lower voltage in subsequent cycles, which implies a rate enhancement in the kinetic process of delithiation of Si nanoparticles.^[20] The CV profiles remain relatively steady after the first cycle, indicating the material has a high reversibility and good stability for the lithiation and delithiation.

The discharge and charge profiles for the first three cycles tested at 100 mA g⁻¹ over a potential window of 0.01–3.5 V are shown in Figure 5b. The first discharge and charge capacities are 1750 and 822 mA h g⁻¹, with the initial Coulombic efficiency reaches 47% only, which is attributed to the formation of SEI layer on the electrode surface and the irreversible electrochemical reactions between Li⁺ and SiO₂ to generate inert phases Li₂O or Li₄SiO₄. The discharge and charge capacity of the second cycle are 900 and 822.6 mA h g⁻¹, with the Coulombic efficiency increases to 91%, and maintained above 95% in the subsequent

cycles. As for the majority of the capacity is delivered at potentials higher than 1.0 V versus Li/Li⁺, Yu and co-workers^[19] proposed that it should be attributed to the large polarization of the glassy material derived from SiO₂. The Si generated during the first conversion cycle has poor conductivity and hinders the kinetics of Li alloying. Chen and co-workers^[29] also claimed that the Li₂O and silicate salts formed during the first discharge process also contribute to the phenomenon because they both have poor electronic conductivity. The same phenomenon can also be observed in HSS electrode (as shown in newly added Figure S2b in the Supporting Information). In order to further verify the possible reason of the high delithiation potential of SiO₂, we compared the charge and discharge curves of HSS-C electrode of different cycles, as shown in Figure 5c, the charge curves become steeper with the increasing of cycling numbers, which is in accordance with the delithiation peak shift in the CV curves, suggesting that the delithiation potential lowers and the hindered Si are slowly activated during cycling.

Figure 6a shows the cycling performance of HSS-C and HSS electrode at 200 mA g⁻¹ for 150 cycles. As we can see, the HSS-C demonstrates a higher reversible capacity and excellent cycling stability, compared with the HSS electrode. The HSS-C electrode delivers an initial charge capacity of ≈780 mA h g⁻¹ and keeps increasing in the following 120 cycles, and thereafter stabilizes to give a specific capacity of 910 mA h g⁻¹ without any tendency of degradation, while the HSS electrode delivers a specific capacity of only 110 mA h g⁻¹. According to the

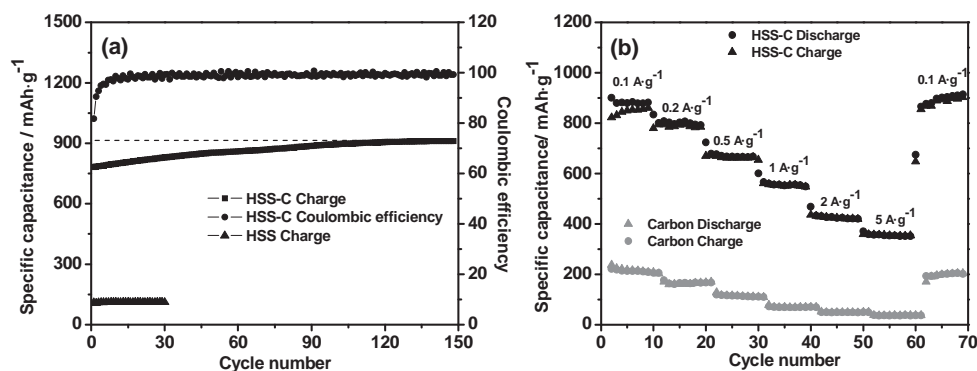


Figure 6. a) Cycling performance of HSS-C and HSS at a current density of 200 mA g⁻¹ and b) rate capability of HSS-C and porous carbon at different current densities.

literature, the resistivity of SiO_2 is as high as $1 \times 10^{13} \Omega \text{ m}$,^[30] which is almost nonconductive. However, the resistivity of amorphous carbon is only $0.35 \Omega \text{ m}$,^[31] with almost 13 orders of magnitude lower than SiO_2 . After coated with carbon on the silica spheres, it is believed that the electrical conductivity of HSS-C can be greatly enhanced. The huge difference of specific capacity confirms the carbon coating plays a remarkable role in enhancing the electrochemical performance of hollow silica spheres as poor conductivity often leads to a low capacity. Considering the 36.5% of carbon in the HSS-C (with the specific capacitance of carbon to be 180 mA h g^{-1} , as shown in Figure 6b), it can be calculated that the specific charge capacity contributed by porous carbon should be about 66 mA h g^{-1} , and the corresponding capacity of SiO_2 should be 1300 mA h g^{-1} . This capacity-climbing phenomenon is common in the field of Li-based rechargeable batteries and can be found in other anodes.^[32–35] There are several possible reasons concerning this phenomenon, first, according to the previously reported works, this “extra capacity” is due to the reversible growth of a polymeric gel-like film resulting from kinetically activated alkyl carbonate electrolyte degradation at low potential.^[32] Moreover, the polymeric gel-like film builds up continually over a number of cycles since the internal surface of active materials is more difficult to access.^[35] Second, it is proposed that the capacity of SiO_2 anode increases over cycles due to the partial reduction of SiO_2 to Si, the growth of the Si phase and, thus, the growth in Si volume. The irreversible formation of Li_4SiO_4 at Si/ SiO_2 interfaces leads to the formation of threefold coordinated Si [Si(III)] outside of its original SiO_4 tetrahedron to bond to the silicon phase, which represents the partial reduction of silica, and turns out to be thermodynamically favorable.^[36] The capacity gained by inclusion of new Si atoms (4 Li per Si) in the Si phase outweighs the loss in capacity due to the consumption of SiO_2 in the irreversible formation of Li_4SiO_4 .^[20,36] The average capacity increase in each cycle is just about 1 mA h g^{-1} , it is reasonable to keep a relative stable Coulombic efficiency over cycles. Similar results were also demonstrated in Zhao's work^[16] and Favors' work.^[20] Besides, a possible reason for the capacity climbing can be due to an activation process of the delayed electrolyte wetting into the 3D nanoporous structure as proposed by other groups for nano-Si anodes.^[37] This may also be similar explanation for our result, as especially for the HSS-C, the hollow silica spheres were completely encapsulated by the porous carbon, the BET specific surface area of HSS-C reaches $297 \text{ m}^2 \text{ g}^{-1}$, which also demonstrates a 3D porous structure. The slow increase in

capacity may also be attributed, at least in part, to the surface activation accompanied with a decreasing charge voltage curve (Figure 5c). More work still needs to be done to give a clear explanation for this phenomenon.

The rate performances at different current densities were evaluated and shown in Figure 6b. From the profiles, HSS-C is found to demonstrate a stable rating behavior, for example, a reversible capacity of $\approx 860 \text{ mA h g}^{-1}$ is achieved at a current density of 100 mA g^{-1} and 560 mA h g^{-1} at a high current density of 1000 mA g^{-1} . The charge capacity returns 915 mA h g^{-1} after the current density returned to 100 mA g^{-1} . The good rate performance of HSS-C is mainly attributed to its refined structure, as mentioned before, the porous carbon with a large specific surface area and pore volume on the surface of silica may facilitate the diffusion and transportation of electrolytes within the electrodes for fast redox reactions during the charge–discharge process even at high current density and at the same time dilute the local current density due to the high specific surface area.^[38]

Scanning electron microscopy (SEM) investigation was also employed to study the structure change of both HSS and HSS-C electrode after 150 charge/discharge cycles, in order to further study the effect of carbon coating in improving the electrochemical performance. As shown in Figure 7a, even the whole particle still retains the spheres morphology in a broad view, but the smooth silica wall was completely destroyed after 150 charge/discharge cycles (as shown in the inset of Figure 7a), compared with that of before cycling (Figure 2a). This phenomenon also suggests that the hollow porous structure of HSS helps to accommodate the structure change during cycling to some extent. However, the hollow silica spheres embedded in porous carbon electrode keeps the same morphology without any fracture, as shown in Figure 7b, which suggests the carbon coated both inside and outside of the hollow structure is crucial to keep the structure stable, which helps to form a relatively stable mixture.

To investigate the influence of carbon coating on the electrochemical kinetics of the Li^+ insertion/extraction process within silica electrodes, electrochemical impedance spectroscopy (EIS) measurement was performed over a frequency range of 100 kHz to 0.01 Hz (see Figure 8a). Figure 8a shows the Nyquist plots of the HSS-C and HSS electrodes after 30 cycles (at 100 mA g^{-1}). Both profiles display a depressed semicircle in the high-frequency region associated with the combined process of surface film (R_f) and the charge transfer resistance (R_{ct}), and a long slope line represents the Warburg impedance (Z_w) at low frequency, which indicates the diffusion of lithium ions

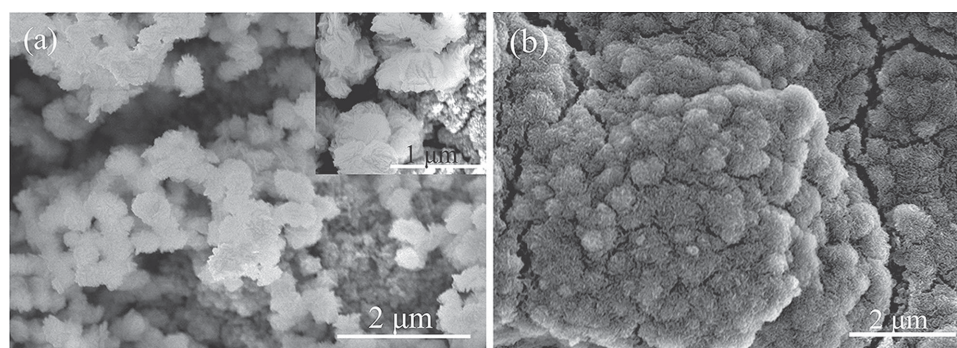


Figure 7. SEM images of the electrodes before cycling and after 150 cycles: a) HSS (inset: large magnification) and b) HSS-C.

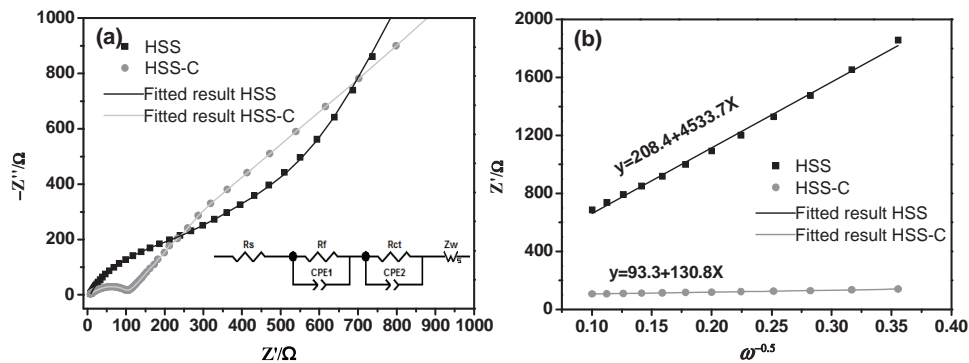


Figure 8. a) EIS plots of HSS–C and HSS at 25 °C (inset: equivalent electrical circuit model) and b) $Z' - \omega^{-0.5}$ plots in the low-frequency range.

in the solid matrix.^[39,40] The plots are fitted with the equivalent electrical circuit model (as shown in the inset of Figure 8a), in which the symbols R_s , R_f , R_{ct} , and Z_w represent the solution resistance, contact resistance, charge-transfer resistance, and Warburg impedance, respectively. The fitting results are shown in Table 1. The R_f and R_{ct} values of HSS-C electrode are 21 and 76 Ω , respectively, which are much smaller than those of the HSS electrode (199 and 280 Ω), suggesting that the carbon coating significantly lowers contact and charge-transfer impedances. Moreover, after the first cycle, silica without carbon coating as a buffer may experience a big volume change and pulverization due to the lithium-ion intercalating into the generated Si particles, thus increasing the contact resistance, charge-transfer resistance. The lithium-ion diffusion coefficient (D_{Li}) could be calculated from the low-frequency plots based on Equation (4) and (5):^[41]

$$Z' = R_e + R_{ct} + \sigma \omega^{-0.5} \quad (4)$$

$$D_{Li} = \frac{(RT)^2}{2(An^2F^2C_{Li}\sigma)^2} \quad (5)$$

In Equation (4), $\omega(2\pi f)$ is the angular frequency in the low-frequency region, R_e represents the $R_s + R_f$, both $R_e + R_{ct}$ and Warburg coefficient (σ) can be obtained from the fitting line while Z' has a linear relationship with $\omega^{-0.5}$. The number of $R_e + R_{ct}$ may be different from the fitting results based on the equivalent circuit, as they are obtained by fitting from the high-frequency area. In Equation (5), T is the absolute temperature, R is the gas constant, A is the surface area of the electrode, n is the number of electrons transfer per mole of the active material involved in the electrode reaction, F is Faraday's constant, and C_{Li} is the molar concentration of Li ions. Based on the linear fitting equation in Figure 8b, the lithium-ion diffusion coefficients of HSS and

HSS–C are calculated to be $\approx 2.81 \times 10^{-19}$ and 3.37×10^{-16} $\text{cm}^2 \text{s}^{-1}$, respectively. Even still lower than the Si-based nanomaterials with a higher conductivity (about 10^{-12} to 10^{-13} $\text{cm}^2 \text{s}^{-1}$),^[42–44] the relatively lower surface film and charge transfer resistance, higher lithium-ion diffusion coefficient, and enhanced electrical conductivity confirm that HSS–C has a more conductive pathway for lithium-ion transportation than bare silica, resulting in enhancement in the electrochemical properties.

The good electrochemical properties of HSS–C electrode could be attributed to several reasons. First, the porous carbon framework with a high pore volume can not only act as an effective electrical highway to enhance the electrical conductivity of HSS–C and a mechanical support to keep all nanoparticles electrochemically active but also act as a matrix, together with the generated lithium salts, that can support and disperse the nano-Si from aggregation and buffer the volume change during Li-ion insertion/extraction in the charging/discharging process,^[16,19,45] which makes great contribution to the excellent cycling performance. Second, the hollow porous structure and the nanosized feature of SiO_2 , and the porous carbon filling in the porous SiO_2 particles prevent fracture and accommodate the mechanical strain during lithiation/delithiation, and thus improve the cycling stability. The porous structure can also reduce the transport distance of electron/lithium ions and offer a large surface for Li-ion reaction. Third, the HSS–C with an enlarged surface area and low charge transfer resistance can facilitate the diffusion and transportation of electrolytes within the electrodes for lithium-ion insertion/extraction, resulting in excellent rate performance. Therefore, benefiting from the unique porous structure and the presence of carbon coating, the HSS–C composite is able to demonstrate excellent reversible capacity, high rate capability, and cyclic stability and shows great potential for application as the next generation of anode materials for high energy high power lithium-ion batteries.

Table 1. Impedance parameters calculated from equivalent circuit.

Sample	R_s [Ω]	R_f [Ω]	R_{ct} [Ω]	D_{Li} [$\text{cm}^2 \text{s}^{-1}$]
HSS	7.3	199	280	2.81×10^{-19}
HSS–C	5.8	21	76	3.37×10^{-16}

3. Conclusion

HSS–C as an anode for lithium-ion batteries was prepared and studied. The synthesized HSS–C shows high specific capacity of 910 mA h g^{-1} at 200 mA g^{-1} , good cycling stability, and rate capability. Not only does the continuous conductive porous

carbon with a large surface area and void space surrounded the silica spheres enhance the electrical conductivity and lithium-ion diffusivity of the electrodes but also help to retain the structural integrity of the electrode and mitigate volume variation during discharge/charge cycles. The intimate contact between porous carbon and silicon nanoparticles in the hollow spheres may also exert some catalytic effect promoting the lithiation and delithiation processes.

4. Experimental Section

Materials: Tetraethylorthosilicate (98 wt%), aqueous ammonia (28 wt%), and ethanol were analytical reagents and purchased from Sigma-Aldrich. Deionized water was used in all the experiments. The resol precursors were prepared according to method reported in the literature.^[21]

Synthesis of HSS-C Composite: First, monodisperse PS spheres with a diameter of ≈ 200 nm (as shown in Figure S1 in the Supporting Information) were synthesized using an emulsion polymerization technique according to the literature.^[23] Second, PS spheres (1.0 g) were added to TEOS-ethanol mixture (20.0 mL) with a weight ratio of 55:45, followed by vacuum filtration and drying in air for 12 h. PS spheres were removed by calcination in air at 575 °C for 8 h to get the hollow silica spheres. Finally, silica spheres (0.8 g) were immersed in a homogeneous ethanol solution (16.0 g) containing resol ($M_w < 500$ g mol⁻¹, 1.0 g) and triblock copolymer P123 (0.5 g). The impregnated composite monoliths were placed to evaporate ethanol at 25 °C for 6 h, followed by further heating at 100 °C for 24 h. The resulting silica/resol/P123 composites were then pyrolyzed in nitrogen at 350 °C for 2 h at a heating rate of 1 °C min⁻¹ to remove P123, and then at 5 °C min⁻¹ rising to 800 °C for 2 h for further carbonization.

Structural Analyses: The crystal structure of the obtained sample was characterized by means of XRD (D8 Bruker X-ray diffractometer with Cu K α radiation ($\lambda = 1.5418$ Å)) within the range of 10–60° (2 θ). The morphology was examined using SEM (FEI, XL30 Sirion FEG). The content of SiO₂ was determined from the weight loss of the sample at 800 °C in air with a TGA apparatus (Q50, TA). Nitrogen sorption isotherms were measured using Quantachrome NOVA 4200e system. Samples were degassed at 200 °C overnight under vacuum prior to measurements. The specific surface area and pore-size distribution were determined by multipoint BET and BJH desorption analyses, respectively.

Electrochemical Measurements: To evaluate the electrochemical performance, a sandwich-type two-electrode testing cell was assembled using the as-prepared samples. The active material was prepared by mixing the HSS-C composites, Super P conductive carbon (TIMCAL Graphite & Carbon), and poly(vinylidene difluoride) (Sigma-Aldrich) binder dispersed in an *N*-methyl-2-pyrrolidone (Alfa Aesar) solution at a weight ratio of 80:10:10, respectively. The as-prepared active material slurry was uniformly spread onto Cu foil and dried in a vacuum oven at 80 °C overnight prior to coin cell assembly. CR2016-type coin cells were assembled in an argon-filled glovebox (Innovative Technology, IL-2GB) with HSS-C composites as the working electrode, pure lithium foil as the counter electrodes, and polypropylene film as the separator (Celgard 2400). The mass loading of the electrode is about 0.8 mg cm⁻². The thickness of the electrode is ≈ 5 μ m and the calculated density of the electrode material is about 1.6 g cm⁻³. 1 M LiPF₆ solution in a volume ratio of 1:1:1 mixture of ethylene carbonate/dimethyl carbonate/dimethyl ethylene carbonate was used as the electrolyte, with 1% VC as the additive. HSS electrode was also prepared in the same way. All electrochemical measurements were performed with the assembled two-electrode battery at ambient temperature. Galvanostatic discharge and charge measurements were performed with LAND CT2001A tester (Wuhan, China) at different current densities in the voltage range of 0.01–3.5 V versus Li/Li⁺. CV was conducted on an electrochemical analyzer (CH Instruments,

model 605 C) in the voltage range of 0.01–2.8 V (vs Li/Li⁺) at a scan rate of 0.1 mV s⁻¹. Alternating current impedance was recorded by applying the Solartron 1287A in conjunction with a Solartron 1260FRA/impedance analyzer with an amplitude of 5.0 mV in the frequency range from 100 kHz to 0.01 Hz.

Supporting Information

Supporting Information is available from the Wiley Online Library or from the author.

Acknowledgements

This work was supported by the National Science Foundation (NSF, DMR-1505902) and by the National Natural Science Foundation of China (Grant No. 51274015). X.C. and S.L. would also like to thank the China Scholarship Council (CSC) for providing a scholarship for Ph.D. study at the University of Washington.

Received: October 27, 2015

Revised: November 25, 2015

Published online: December 28, 2015

- [1] Q. Zhang, E. Uchaker, S. L. Candelaria, G. Cao, *Chem. Soc. Rev.* **2013**, *42*, 3127.
- [2] J. B. Goodenough, K. S. Park, *J. Am. Chem. Soc.* **2013**, *135*, 1167.
- [3] F. Cheng, J. Liang, Z. Tao, J. Chen, *Adv. Mater.* **2011**, *23*, 1695.
- [4] Y. Wang, H. Li, P. He, E. Hosono, H. Zhou, *Nanoscale* **2010**, *2*, 1294.
- [5] J. B. Goodenough, Y. Kim, *Chem. Mater.* **2010**, *22*, 587.
- [6] H. Wu, Y. Cui, *Nano Today* **2012**, *7*, 414.
- [7] H. Wu, G. Chan, J. W. Choi, I. Ryu, Y. Yao, M. T. McDowell, S. W. Lee, A. Jackson, Y. Yang, L. Hu, Y. Cui, *Nat. Nanotechnol.* **2012**, *7*, 310.
- [8] L. F. Cui, Y. Yang, C. M. Hsu, C. Yi, *Nano Lett.* **2009**, *9*, 3370.
- [9] N. Yan, F. Wang, H. Zhong, Y. Li, Y. Wang, L. Hu, Q. W. Chen, *Sci. Rep.* **2013**, *3*, 6.
- [10] B. K. Guo, J. Shu, Z. X. Wang, H. Yang, L. H. Shi, Y. N. Liu, L. Q. Chen, *Electrochem. Commun.* **2008**, *10*, 1876.
- [11] X. Q. Yang, H. Huang, Z. H. Li, M. L. Zhong, G. Q. Zhang, D. C. Wu, *Carbon* **2014**, *77*, 275.
- [12] Y. Zhu, C. Cao, J. Zhang, X. Xu, *J. Mater. Chem. A* **2015**, *3*, 9556.
- [13] S. Wu, Z. Wang, C. He, N. Zhao, C. Shi, E. Liu, J. Li, *J. Mater. Chem. A* **2011**, *1*, 11011.
- [14] M. Zhang, E. Uchaker, S. Hu, Q. Zhang, T. Wang, G. Cao, J. Li, *Nanoscale* **2013**, *5*, 12342.
- [15] H. Takezawa, K. Iwamoto, S. Ito, H. Yoshizawa, *J. Power Sources* **2013**, *244*, 149.
- [16] P. P. Lv, H. L. Zhao, J. Wang, X. Liu, T. H. Zhang, Q. Xia, *J. Power Sources* **2013**, *237*, 291.
- [17] J. Shu, R. Ma, M. Shui, D. J. Wang, N. B. Long, Y. L. Ren, R. F. Zhang, J. H. Yao, X. B. A. Mao, W. D. Zheng, S. Gao, *RSC Adv.* **2012**, *2*, 5806.
- [18] W. S. Chang, C. M. Park, J. H. Kim, Y. U. Kim, G. Jeong, H. J. Sohn, *Energy Environ. Sci.* **2012**, *5*, 6895.
- [19] Y. Yao, J. J. Zhang, L. G. Xue, T. Huang, A. S. Yu, *J. Power Sources* **2011**, *196*, 10240.
- [20] Z. Favors, W. Wang, H. H. Bay, A. George, M. Ozkan, C. S. Ozkan, *Sci. Rep.* **2014**, *4*, 7.
- [21] H. J. Liu, W. J. Cui, L. H. Jin, C. X. Wang, Y. Y. Xia, *J. Mater. Chem.* **2009**, *19*, 3661.

- [22] K. S. W. Sing, D. H. Everett, R. A.W. Haul, L. Moscou, R. A. Pierotti, J. Rouquerol, T. Siemieniewska, *Pure Appl. Chem.* **1985**, *57*, 603.
- [23] Y. J. Du, M. Y. Hou, D. D. Zhou, Y. G. Wang, C. X. Wang, Y. Y. Xia, *J. Energy Chem.* **2014**, *23*, 315.
- [24] C. Guo, D. Wang, T. Liu, J. Zhu, X. Lang, *J. Mater. Chem. A* **2014**, *2*, 3521.
- [25] H. X. Gong, N. Li, Y. T. Qian, *Int. J. Electrochem. Sci.* **2013**, *8*, 9811.
- [26] T. Doi, M. Tagashira, Y. Iriyama, T. Abe, Z. Ogumi, *J. Appl. Electrochem.* **2012**, *42*, 69.
- [27] Q. Sun, B. Zhang, Z. W. Fu, *Appl. Surf. Sci.* **2008**, *254*, 3774.
- [28] J. Wang, H. L. Zhao, J. C. He, C. M. Wang, *J. Power Sources* **2011**, *196*, 481.
- [29] M. Li, Y. Yu, J. Li, B. Chen, X. Wu, Y. Tian, P. Chen, *J. Mater. Chem. A* **2015**, *3*, 1476.
- [30] J. K. Srivastava, M. Prasad, J. B. Wagner, *J. Electrochem. Soc.* **1985**, *132*, 955.
- [31] M. Sharif Md, K. Kalaga Murali, S. Tetsuo, J. Takashi, U. Masayoshi, *Jpn. J. Appl. Phys.* **1999**, *38*, 658.
- [32] Z. Zeng, H. Zhao, P. Lv, Z. Zhang, J. Wang, Q. Xia, *J. Power Sources* **2015**, *274*, 1091.
- [33] F. Ma, A. Yuan, J. Xu, *ACS Appl. Mater. Interfaces* **2014**, *6*, 18129.
- [34] J. Zhu, Z. Yin, D. Yang, T. Sun, H. Yu, H. E. Hoster, H. H. Hng, H. Zhang, Q. Yan, *Energy Environ. Sci.* **2013**, *6*, 987.
- [35] L. Hu, H. Zhong, X. Zheng, Y. Huang, P. Zhang, Q. Chen, *Sci. Rep.* **2012**, *2*, 986.
- [36] C. Ban, B. B. Kappes, Q. Xu, C. Engrakul, C. V. Ciobanu, A. C. Dillon, Y. Zhao, *Appl. Phys. Lett.* **2012**, *100*, 243905.
- [37] H. Wu, G. Yu, L. Pan, N. Liu, M. T. McDowell, Z. Bao, Y. Cui, *Nat. Commun.* **2013**, *4*, 1943.
- [38] P. Lv, H. Zhao, C. Gao, T. Zhang, X. Liu, *Electrochim. Acta* **2015**, *152*, 345.
- [39] M. E. Orazem, B. Tribollet, *Electrochemical Impedance Spectroscopy, The Electrochemical Society Series*, John Wiley & Sons Inc, Hoboken, NJ, USA, **2008**, p. 153.
- [40] S. S. Zhang, K. Xu, T. R. Jow, *Electrochim. Acta* **2004**, *49*, 1057.
- [41] Y. F. Deng, S. X. Zhao, Y. H. Xu, C. W. Nan, *J. Mater. Chem. A* **2014**, *2*, 18889.
- [42] N. Ding, J. Xu, Y. X. Yao, G. Wegner, X. Fang, C. H. Chen, I. Lieberwirth, *Solid State Ionics* **2009**, *180*, 222.
- [43] J. Li, N. J. Dudney, X. Xiao, Y.-T. Cheng, C. Liang, M. W. Verbrugge, *Adv. Energy Mater.* **2015**, *5*, 1401627.
- [44] T. Zhang, L. J. Fu, J. Gao, L. C. Yang, Y. P. Wu, H. Q. Wu, *Pure Appl. Chem.* **2006**, *78*, 1889.
- [45] W. R. Liu, Y. C. Yen, H. C. Wu, M. Winter, N. L. Wu, *J. Appl. Electrochem.* **2009**, *39*, 1643.